Gaussian Decomposition of Laser Altimeter Waveforms

Michelle A. Hofton, J. Bernard Minster, and J. Bryan Blair.

M. A. Hofton is with the Department of Geography, University of Maryland, College Park, MD 20742 USA (e-mail: mhofton@geog.umd.edu)

J.-B. Minster is with the Institute of Geophysics and Planetary Physics, Scripps Institution of Oceanography, La Jolla, CA 92093 USA (e-mail: jbminster@ucsd.edu)

J. B. Blair is with NASA's Goddard Space Flight Center, Code 924, Greenbelt, MD 20771 USA (e-mail: bryan@avalon.gsfc.nasa.gov)

Abstract

We develop a method to decompose a laser altimeter return waveform into its Gaussian components assuming that the position of each Gaussian within the waveform can be used to calculate the mean elevation of a specific reflecting surface within the laser footprint. We estimate the number of Gaussian components from the number of inflection points of a smoothed copy of the laser waveform, and obtain initial estimates of the Gaussian half-widths and positions from the positions of its consecutive inflection points. Initial amplitude estimates are obtained using a non-negative least-squares method. To reduce the likelihood of fitting the background noise within the waveform and to minimize the number of Gaussians needed in the approximation, we rank the "importance" of each Gaussian in the decomposition using its initial half-width and amplitude estimates. The initial parameter estimates of all Gaussians ranked "important" are optimized using the Levenburg-Marquardt method. If the sum of the Gaussians does not approximate the return waveform to a prescribed accuracy, then additional Gaussians are included in the optimization procedure. The Gaussian decomposition method is demonstrated on data collected by the airborne Laser Vegetation Imaging Sensor (LVIS) in October 1997 over the Sequoia National Forest, California.

Keywords

Laser altimetry, gaussian decomposition, surface-finding, data processing

I. Introduction

Laser altimetry is a powerful remote sensing technique, poised to provide unique information on surface elevations and ground cover to the Earth science community. The measurement concept is simple: a laser altimeter records the time of flight of a pulse of light from a laser to a reflecting surface and back. This travel time, combined with ancillary information such as laser location and pointing at the time of each laser shot, enables the laser footprint to be geolocated in a global reference frame. Digitally recording the return laser pulse shape provides information on the elevations and distributions of distinct reflecting surfaces within the laser footprint.

Early laser altimeter systems were flown onboard the Apollo 15, 16 and 17 missions to the Moon in the 1970's [1]. More recently, laser altimeters flown in space include the Shuttle Laser Altimeter (SLA) [2], and the Mars Orbital Laser Altimeter (MOLA) [3], both missions demonstrating that meter-level topography of the Earth and other planets is routinely obtainable using the technique. Recent advances in ranging and processing techniques and the digital recording of the return laser pulse shape in airborne systems

such as the Laser Vegetation Imaging Sensor (LVIS) [4] show decimeter-level of accuracy is now obtainable [5]. Building on this heritage, the next generation of spaceborne and airborne laser altimeter systems seek to monitor a diverse range of geophysical phenomena at unprecedented levels of precision and accuracy. These systems include the Geoscience Laser Altimeter System (GLAS) [6], which will measure ice sheet elevation changes with decimeter-level accuracy, and the Vegetation Canopy Lidar (VCL) [7] which will determine tree height and vertical structure and sub-canopy topography with meter-level accuracy.

Critical to the success of both the GLAS and VCL missions is the ability to understand and interpret the shape of the digitally-recorded return laser pulse to extract timing points for specific reflecting surfaces within the footprint (e.g., first and last), and thus directly to geolocate the desired reflecting surface. A digitally-recorded return laser pulse, or waveform (Fig. 1), represents the time history of the laser pulse as it interacts with the reflecting surfaces. (Note that the waveform does not represent a continuous function but rather a set of equally-spaced digitized samples from the return energy distribution.) The waveform can have a simple (single-mode) shape, similar to that of the outgoing pulse (Fig. 1a), or be complex and multi-modal with each mode representing a reflection from a distinct surface within the laser footprint (Fig. 1b). Simple waveforms are typical in ocean or bare-ground regions, and complex waveforms in vegetated regions. The temporally-first and last modes within the waveform are associated with the highest and lowest reflecting surfaces within the footprint respectively.

To consistently geolocate the desired reflecting surface, for example, the underlying ground surface in vegetated regions, we need to be able to precisely identify the corresponding reflection within the waveform. Existing waveform processing methods generally do not take into account surface type nor its effect on the shape of the return laser pulse, and thus do not provide a consistent ranging point to a reflecting surface during data processing. These methods include finding the location of the peak amplitude within the waveform or the location of the centroid of the return waveform. For a simple waveform, i.e., the pulse is represented by a single Gaussian distribution, both of these methods reliably locate the reflecting surface of interest (Fig. 1a). However, for complex waveforms, i.e., waveforms containing several Gaussian distributions, the reflecting surface of interest

may not reflect the maximum amplitude return, and clearly, the centroid of the waveform is unlikely to represent accurately the desired reflecting surface elevation (Fig. 1b). Thus, to locate a reflecting surface consistently within a laser altimeter waveform, we seek to decompose a return waveform into Gaussian components, the sum of which can be used to approximate the waveform. We assume that each Gaussian represents the reflected distribution of laser energy from a reflecting surface within the footprint, and that the location of the center of each Gaussian can be used to geolocate the reflecting surface of interest in the vertical direction.

II. Statement of the Problem

Given a sequence of uniformly-spaced points $\{x_k\colon\ k=1,...N\}$ with associated data values $\{y_k\colon\ k=1,...N\}$, we wish to decompose a return waveform into its Gaussian components in the form

$$y = f(x) = \sum_{i=1}^{n} a_i\, e^{-(x-x_i)^2/2\sigma^2}, \tag{1}$$

such that

$$\sqrt{\frac{1}{N}\sum_{k=1}^{N}(f(x_k) - y_k)^2} < \epsilon. \tag{2}$$

$y = f(x)$ is a single-valued curve with parameters $\{a_i, x_i, \sigma_i\}$ for $i=1,...n$, determined so that the curve fits the data with prescribed accuracy ϵ using some number of Gaussians, n. The amplitude, position and half-width of each Gaussian are denoted by a_i, x_i,and σ_i respectively.

This problem is described by a system of $3n$ non-linear equations, and can be solved using a non-linear least-squares method such as the Levenburg-Marquardt technique [8] which minimizes the weighted sum of squares between the observed waveform and its Gaussian decomposition. A consequence of using the Levenburg-Marquardt technique, however, is that we must provide a realistic set of initial Gaussian parameters in order to limit the likelihood of the least-squares-derived solution ending up in a local minima. We thus estimate the number of Gaussian components within the waveform from the number of inflection points of a smoothed (i.e, filtered so as to remove high frequency noise) copy of the waveform. Initial position and half-width estimates for each component Gaussian are derived from the locations and separations of consecutive inflection points. Initial

amplitude parameters for all component Gaussians are then simultaneously estimated using a non-negative least-squares method.

The optimized parameters generated by the Levenburg-Marquardt technique represent a series of Gaussians, the sum of which can be used to approximate the waveform. The sum of the Gaussians is considered to be a reasonable representation of the laser waveform if the residual differences between the sum of the Gaussians and the observed waveform resemble the background noise in the waveform. The statistics of the fit are governed by the particular application of the waveform data. In this study, our criterion was that the standard deviation of the residual difference, σ_r, must be less than three times the standard deviation of the background noise within the observed waveform, σ_n. In the notation of equation (2), this implies $\epsilon = 3\sigma_n$.

III. The Fitting Algorithm

A. Identify Number of Gaussians

We derive the number of Gaussians needed to approximate the observed waveform from the number of inflection points of the observed waveform. We use the fact that a single Gaussian has two inflection points and that when n Gaussians are combined there will be $2n$ inflection points at most. Difficulties arise when two neighboring Gaussians are close enough together that only two inflection points (instead of four) are detected, making it impossible to isolate the close Gaussian pair. Random amplitude changes within the waveform background noise will also cause inflection points. This leads to the false detection of spurious Gaussians within the portion of the waveform that in reality does not contain reflected signal. To minimize this problem, we smooth the observed waveform to reduce high-frequency noise before locating its inflection points. The smoothing is performed by convolving a Gaussian of some predetermined half-width with the observed waveform. The choice of the half-width of the smoothing Gaussian must be tailored to the data set and laser altimeter under study. We base our choice on the half-width of the impulse response of the system (i.e., the half-width of the laser pulse as seen through the detector and recording system). If this half-width is unknown, then the half-width of the return laser pulse (at a normal incidence angle) over a flat surface such as the ocean can

be used.

Fig. 2 shows a simulated laser altimeter return waveform from complex terrain and the effect of smoothing it with a Gaussian filter. The waveform was generated from the sum of three Gaussians sampled at discrete time bins. We assume each Gaussian represents the distribution of laser energy reflected from a distinct vertical layer within the laser footprint, e.g., tree top, underlying vegetation and the ground. Random (normally-distributed) noise was superimposed on the sum of the three Gaussians simulating background noise introduced by the digitizer. The simulated return samples were rounded to integer amplitude values in order to simulate the effect of digitizer sampling.

As the half-width of the smoothing Gaussian is increased, the signal within the waveform is broadened and returns from reflecting surfaces become less distinct (Fig. 2). Using a smoothing filter half-width of 5 bins results in a total of 24 inflection points, implying there are at most twelve Gaussian components within the waveform. However, the majority of these are associated with the background noise within the waveform. These will be easily identified and discarded from the optimization in subsequent steps.

B. Generate Initial Parameter Estimates

We generate initial estimates for the positions and half-widths of the Gaussian components within an observed waveform from the positions of the inflection points of a smoothed version of the observed waveform, and assume (for simplification) that consecutive inflection points belong to the same Gaussian. Using the positions of consecutive inflection points, l_{2i-1} and l_{2i}, the position, x_i, and half-width, σ_i, of the i^{th} Gaussian are given by

$$x_i = (l_{2i-1} + l_{2i})/2, \tag{3}$$

$$\sigma_i = |l_{2i-1} - l_{2i}|/2. \tag{4}$$

The corresponding initial amplitudes are estimated using a non-negative least-squares method [9]. We use a non-negative least-squares method, constraining the Gaussian amplitudes to be greater than zero because the returning intensity distributions must have positive amplitudes. The non-negative least-squares problem solves the system of equations

$$Ea = b \tag{5}$$

in a least-squares sense subject to the constraint that the solution vector, a, have only non-negative elements [9]. The vector, a, contains the initial amplitude estimates of the n Gaussians. Details of the algorithm are found in *Lawson and Hanson* [1974]. Initial parameter estimates for the Gaussian components of our simulated waveform (Fig. 2) are given in Table I.

We also estimate the mean background noise level, m, within the waveform. If statistics on the background noise level are not available directly, then an initial estimate for the simulated waveform (Fig. 2) is easily obtained from the background noise in a region of the original waveform where no signal is expected: for this particular example we use the last 10 bins of the waveform. The standard deviation of the mean background noise, σ_n, used to determine the accuracy of the final approximation, is also determined in this step. σ_n is 0.68 bins.

C. Flag and Rank Gaussians in Order of Importance

The use of the number of inflection points within a smoothed copy of the observed waveform identifies many putative Gaussian components within the waveform, the majority of which are associated with random background noise. We minimize the number of Gaussians used for the decomposition of the observed waveform by a flagging and ranking procedure. We flag Gaussians with initial half-width estimates greater than or equal to the half-width of the laser impulse response and with initial amplitudes estimates greater than three times the standard deviation of the mean noise level, σ_n, as "important". We rank remaining Gaussians by their positions relative to the position of an "important" Gaussian; the shorter the distance from the position of the Gaussian to the position of an "important" Gaussian, the higher it is ranked. Gaussians flagged "important" are used first in the optimization step. Ranked Gaussians are included in the optimization only if the optimal fit statistic suggests more Gaussians are required.

This procedure attempts to prevent the decomposition of the background noise within the observed waveform into Gaussian components, as well as reduce the likelihood of overinterpreting the observed waveform by minimizing the number of Gaussians needed for the decomposition. For the example waveform shown in Fig. 2, three out of the twelve Gaussians detected (Table I) meet the selection criteria and are flagged as important for

the parameter optimization step. The remaining Gaussians are ranked by their location within the waveform.

D. Perform Parameter Optimization

We perform parameter optimization using a non-linear least-squares method. A variety of such techniques exist which find solutions by iteratively trying a series of combinations of the parameters until a solution is found. Problems occur when the fit ends up in a local minimum, which may not be the best possible solution, or if the initial estimates are significantly far from the true answer. We use a constrained version of the Levenburg-Marquardt technique [8], one of the most-widely used non-linear fitting techniques, and coded implementations of which are freely available (we use an implementation written for the Interactive Data Language (IDL) package and translated from MINPACK-1 [10]). The Levenburg-Marquardt technique uses the method of steepest descent to determine the step size when the results are far from the minimum, then switches to the Newton method to determine the step size in order to determine the best fit. It requires that the first derivatives of the minimizing function be known. The derivatives are easily calculated from equation (1). See [8] for further details on this technique.

To restrict the outcome of the optimization to reasonable estimates, we constrain the optimized amplitudes and half-widths of the component Gaussians to be positive and greater than or equal to the half-width of the laser impulse response respectively. The Gaussian components must also be located within the extent of the waveform. All other parameters are assumed free and unconstrained. Within these bounds the technique finds the set of parameters that best fits the data. The fit is best in a least-squares sense, i.e., we minimize the sum of the squared differences between the model and data. Thus, if w are the one-sigma uncertainties in the observations, y, then the technique seeks to minimize the χ^2 value given by

$$\chi^2 = \sum \left[\frac{y_i = f(x_i)}{w_i} \right]^2 . \tag{6}$$

For the example waveform shown in Fig. 2, parameter optimization is initially performed on the three Gaussians components flagged as "important" in Step C. Table II shows the optimized parameters of these three Gaussians derived by the Levenburg-Marquardt tech-

nique to approximate the waveform. The original and approximated waveform, composed of the sum of the component Gaussians are shown in Fig. 3a. The residuals of the fit are shown in Fig. 3b. The mean and standard deviation of the residuals are -0.03 bins and 0.82 bins respectively. The standard deviation is less than three times the standard deviation of the background noise of the observed waveform (0.68 bins), thus, this fit is considered reasonable. If the predefined accuracy criteria are not met, this may imply that more Gaussians are required to approximate the waveform or that the fit has ended up in a local minimum. In this case, the optimization is repeated including the remaining, highest-ranked Gaussian from Step C or using recalculated parameter estimates.

E. The Algorithm

The following algorithm decomposes a laser altimeter return waveform into a series of Gaussians.

Method:

1. Smooth (so as to improve the signal to noise ratio) a copy of the observed waveform with a Gaussian of predefined half-width, and isolate its inflection points. Suppose $2p$ inflection points are found, implying the waveform will be decomposed into at most p Gaussians.
2. Estimate the parameters of the p Gaussians using equations (3)-(5), along with the mean background noise level.
3. Flag and rank Gaussians in order of importance using predefined half-width and amplitude criteria. Suppose n Gaussians are flagged important.
4. Use the parameter estimates of the n flagged Gaussians and the estimate for the mean background noise level as the initial values for the Levenburg-Marquardt technique and refine the parameters by minimizing the χ^2 measure of misfit between the observed and approximated waveform.
5. Suppose the error obtained by the Levenburg-Marquardt technique using n Gaussians is e_n. If $e_n < \epsilon$ stop, otherwise increment n by one (up to a maximum of p) or recalculate the initial parameter estimates and go to step 4.

Using this algorithm, the most-important Gaussians are identified, then used in the approximation. If the prescribed accuracy is not reached, then the number of Gaussians

is increased by one at each iteration or the initial parameter estimates are recalculated. The algorithm will stop at step 4 if the sum of all p Gaussians prove insufficient to approximate the data to the prescribed accuracy. In this case, the fit has likely ended up in a local minimum, and the initial parameter estimates should be recalculated carefully. The parameters of the Gaussian components of a laser altimeter waveform can be used to vertically-locate reflecting surfaces of interest, as well as being used for other scientific investigations.

IV. Application of the Algorithm to Observed Data

We demonstrate the algorithm for the decomposition of laser altimeter waveforms into a series of Gaussians on data collected by the Laser Vegetation Imaging Sensor (LVIS) [4]. LVIS is a medium altitude airborne laser altimeter, nominally operating up to 8 km above ground level and acquiring a 1000 m-wide data swath. The system digitally records the shape of both the outgoing and return laser pulses through the full detector and digitizer chain, so that the impulse response of the system is recorded at each epoch. In October 1997, LVIS was operated in NASA's T39 jet aircraft from ~6 km above the Sequoia National Forest in southeast California (Fig. 4). The laser fired at 400 Hz to generate thirty-five across track footprints, each ~20 m in diameter and separated by ~10 m both along and across track (Fig. 4).

Fig. 5a shows a typical, digitized outgoing laser pulse from the altimeter during the LVIS mission. Using the decomposition algorithm, we can easily approximate the pulse by a single Gaussian of half-width 2.5 bins (note, each bin represents 2 ns in time [4]). A Gaussian of half-width 3 bins was used to smooth the waveform. The digitized return pulse for this laser shot is shown in Fig. 5b. The waveform is complex, due to the interactions of the laser pulse with the tall, multi-storied pine trees in the region. Using the decomposition algorithm, we required five Gaussian components to approximate the return (Fig. 5b), presumably representing four distinct layers within the canopy and the underlying ground. The number of Gaussian components within the return waveform may indicate the complexity of the surface structure within the laser footprint. Furthermore, the Gaussians approximating the interaction of the laser pulse with the canopy layers are wider and lower in amplitude than the Gaussian approximating the interaction of the laser

pulse with the ground. This may indicate that the canopy layers are spread over a large vertical extent, and that the canopy is relatively open since most of the energy of the return waveform is contained within the ground response.

Existing laser altimetry processing techniques (e.g., [11]) allow us to convert the waveform time bins into elevation bins. For the LVIS system during this flight, one waveform time bin (2 ns) is equivalent to 0.2997 m in one-way corrected range along the laser beam path [4]. If we assume the position of each Gaussian within the waveform (Table III) locates the center of each reflecting layer and the position of the last Gaussian represents the ground, then the canopy layers at this footprint location are at mean heights of 68.52 m, 60.78 m, 47.08 m and 35.19 m above the ground.

A method to assess the uniqueness of this interpretation might involve looking at consistency from waveform to waveform for some or most of the Gaussian components. Fig. 6 shows the waveforms from the footprints surrounding the footprint in Fig. 5. The waveforms are vertically-geolocated relative to the WGS-84 ellipsoid (i.e., the elevation of each mode in the waveform is relative to the ellipsoid, not to the ground). This type of geolocated waveform is a typical data product of laser altimeter systems such as LVIS, SLA and VCL. The shape of each waveform varies from footprint to footprint (Fig. 6), changing from simple and single mode (Fig. 6a) to complex and multi-modal (Fig. 6c) within a distance of about 20 m. However, some consistency in the waveform shapes is evident, e.g., the mode representing the ground response occurs at about 2090 m above the ellipsoid in all the waveforms indicating that the ground is relatively flat at this location.

Using the decomposition algorithm, each waveform ends up being decomposed into its Gaussian components (keeping the vertical alignment of the waveforms in the WGS-84 reference system). Each waveform is decomposed into a different number of components, however, there is consistency in the vertical locations of some of the Gaussian components from footprint to footprint (Fig. 6). For example, Gaussians are consistently located at elevations of ~2155 m in Figs. 6c–d, at ~2147 m in Figs. 6b–d, at ~2135 m in Figs. 6c–e, at ~2122 m in Figs. 6d–f and at ~2107 m in Figs. 6e–f. This indicates that the algorithm is consistently locating reflecting surfaces shot-to-shot perhaps allowing a unique interpretation of canopy heights and surface elevations in this region.

V. Discussion

The decomposition of an observed laser altimeter waveform into Gaussian components not only allows the determination of the heights of various reflecting surfaces within the laser footprint, but may also allow us to quantify such parameters as landscape complexity and canopy openness within the footprint. These can be determined from the number of component Gaussians and their relative amplitudes and half-widths. However, the outcome of the approximating algorithm is likely non-unique, and furthermore, influenced by several decisions, including our choice of optimization technique and least-squares fitting criteria, and the initial estimates for the number and parameters of the Gaussians needed to approximate the waveform. It should be noted that this is not the only method by which a 1-dimensional signal can be decomposed into a sum of Gaussians. Many other optimization techniques exist, and initial parameter estimates can be generated using methods such as scale-space analysis [12]. Consideration must be made, however, of the physical interaction of the laser beam with the reflecting surface, for example, the scale-space analysis technique does not restrict the initial amplitude estimates to be positive, a physically unreasonable situation.

The use of the Levenburg-Marquardt technique also allows us easily to change the nature of the expected retun pulse distribution. Observed waveforms of existing laser altimeter systems reveal that the laser impulse response is very rarely truly Gaussian in nature, for example, the outgoing pulse for the LVIS instrument during the Sequoia mission was slightly asymmetric, containing a ramp on the back-end of the pulse (Fig. 5). This has implications for the return laser pulse shape since over a flat surface at nadir intercept angle, the return pulse will mirror the shape of the outgoing pulse. Approximating these waveforms using a sum of Gaussians may not be an accurate representation, depending on the application. For these cases, we can use a better approximation of the shape of the impulse response in the optimization, for example, two exponential curves with different decay times.

We are able to restrict the outcome of the Levenburg-Marquardt algorithm using constraints on the half-width and amplitudes on the component Gaussians. Other constraints on the parameters of the component Gaussians can also be imposed, based upon land-

scape characteristics (e.g., in flat terrain, return pulses cannot be wider than the impulse response of the system), or context provided by the decomposition of the preceding and following laser footprints (e.g., we can trace the ground elevation from footprint to footprint to verify consistency (Fig. 6)). These constraints could aid in limiting the number of possible outcomes of the Gaussian decomposition process, thus improving our accuracy of predicting landcover features over large areas from laser altimeter waveforms.

VI. Summary

An algorithm has been created to decompose a laser altimeter return waveform from simple and complex surfaces into a series of Gaussians. We assume each Gaussian relates to the distribution of laser energy returned from a distinct reflecting surface within the laser footprint, and can be used to obtain the elevation of the reflecting surface. In use on waveform data recorded by the LVIS airborne altimeter system at the Sequoia National Forest in California, the algorithm consistently locates the ground beneath the overlying canopy. The algorithm also easily allows any other distinct reflecting surface layers within the footprint to be vertically-located using the position of each approximating Gaussian. The use of this algorithm will allow us to utilize the full potential of waveform data collected by spaceborne and airborne laser altimeters such as the VCL, GLAS, and LVIS systems, insofar that we can consistently locate a desired reflecting surface such as bare ground under different land cover conditions, and obtain precise elevation measurements of several reflecting surfaces within the laser footprint.

Acknowledgments

This work was supported by NASA under Grant NAGS-3001, and by the Geoscience Laser Altimeter System Science Team under Contract Number NAS5-33019.

References

[1] W. M. Kaula, G. Schubert, R. E. Longenfelter, W. L. Sjorgen, and W. R. Wollenhaupt, "Apollo laser altimetry and inferences as to lunar structure", *Geochim. Cosmochim. Acta, 38, 3049-3058*, 1974.

[2] J. B. Garvin, J. Bufton, J. Blair, D. Harding, S. Luthcke, J. Frawley, and D. Rowlands, "Observations of the Earth's topography from the Shuttle Laser Altimeter (SLA): Laser pulse echo-recovery measurements of terrestrial surfaces", *Phys. Chem. Earth, 23*, 1053-1068, 1998.

[3] D. E. Smith, M. T. Zuber, H. V. Frey, J. B. Garvin, J. W. Head, D. O. Muhleman, G. H. Petengill, R. J. Phillips, S. C. Solomon, H. J. Zwally, W. B. Banerdt, and T. C. Duxbury, "Topography of the northern hemisphere of Mars from the Mars Orbiter Laser Altimeter", *Science, 279, 1686–1692*, 1998.

[4] J. B. Blair, D. L. Rabine, and M. A. Hofton, "The Laser Vegetation Imaging Sensor (LVIS): A medium altitude, digitization only, airborne laser altimeter for mapping vegetation and topography", *ISPRS J. Photogramm. Rem. Sens., 54, 115-122*, 1999.

[5] M. A. Hofton, J.-B. Minster, J. R. Ridgway, N. P. Williams, J. B. Blair, D. L. Rabine, and J. L. Bufton, "Using Airborne Laser Altimetry to Detect Topographic Change at Long Valley Caldera, California," to appear in *AGU Monograph: Remote Sensing of Volcanoes*, ed. P. Mouginis-Mark, 1999.

[6] S. Cohen, J. Degnan, J. Bufton, J. Garvin, and J. Abshire, "The geoscience laser altimetry/ranging system", *IEEE Trans. Geosci. Remote Sens., 25, 581–592*, 1987.

[7] R. Dubayah, J. B. Blair, J. L. Bufton, D. B. Clark, J. Ja Ja, R. Knox, S. B. Luthcke, S. Prince, and J. Weishampel, "The Vegetation Canopy Lidar mission", *Land Satellite Information in the Next Decade II: Sources and Applications*, American Society for Photogrammetry and Remote Sensing, 100–112, 1997.

[8] D. Marquardt, "An algorithm for least squares estimation of non-linear parameters", *J. Soc. Indust. Appl. Math., 11, 431–441*, 1963.

[9] C. L. Lawson, and R. J. Hanson, *Solving Least Squares Problems*, pp. 340, Prentice-Hall, 1974.

[10] C. Markwardt, *Curve fitting in IDL using MPFITEXPR*, http://astrog.physics.wisc.edu/ craigm/idl/ - fittut.html, 1998.

[11] M. A. Hofton, J. B. Blair, J.-B. Minster, J. R. Ridgway, N. P. Williams, J. L. Bufton, and D. L. Rabine, "An airborne scanning laser altimetry survey of Long Valley, California", in press *Intl. J. Rem. Sens.*, 1999.

[12] A. P. Witkin, "Scale space filtering: A new approach to multi-scale description", *Image Understanding, 79–95*, 1984.

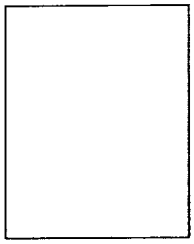

Michelle Hofton received the B.Sc. degree in Natural Sciences and the Ph.D. in Geophysics from the University of Durham, England in 1991 and 1995. She was with the Institute of Geophysics and Planetary Physics, Scripps Institution of Oceanography, La Jolla, California from 1995 to 1998, where she worked on developing precision geolocation algorithms to process laser altimetry data and was involved with using airborne laser altimetry to measure topographic change at Long Valley caldera, CA. She was also involved with applying airborne techniques for the benefit of the Geoscience Laser Altimeter System (GLAS). She is now at the University of Maryland, College Park involved with the calibration and validation of the Vegetation Canopy Lidar (VCL).

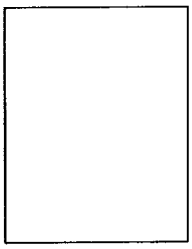

Jean-Bernard Minster is the systemwide director of the Institute of Geophysics and Planetary Physics (IGPP) of the University of California and senior fellow at SDSC. He is a professor in IGPP at Scripps Institution of Oceanography. He obtained his B.S. in mathematics from the Academie de Grenoble and graduated as a civil engineer from the Ecole des Mines, Paris, and as a petroleum engineer from the Institut Francais du Petrole (1969). He obtained his Ph.D. (1974) in geophysics from the California Institute of Technology and, in the same year, a doctorate in physical sciences from the Universite de Paris VII. Professor Minster's research interests are centered around the determination of the structure of the Earth's interior from broad-band seismic data, by imaging the Earth's upper mantle and crust using seismic waves. This research has led him to an involvement in the use of seismic means for verification of nuclear test ban treaties. He has long been interested in global tectonic problems and more recently in the application of space-geodetic techniques, including synthetic aperture radar and laser altimetry, to study tectonic and volcanic deformations of the earth's crust. Using similar techniques, he has also proposed improvements of ship and airborne measurements of the Earth's gravity field. His continued interest in nuclear monitoring has recently led him to study ionospheric disturbances caused by earthquakes, mining blasts and other explosions, and rockets, using the Global Positioning System. He is also pursuing research on the validation of earthquake prediction methods based on pattern recognition techniques. His teaching has centered on plate tectonics and plate deformation, seismology, and on the use of space geodesy to study the Earth and how it changes with time. He has held positions in industry and has been a consultant and reviewer for numerous companies. He was the Nordberg Lecturer at NASA/GSFC in 1996 and was elected a Fellow of the American Geophysical Union in 1990.

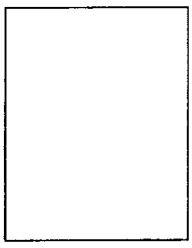

Bryan Blair received the B.Sc. degree in Pure Mathematics from Towson University, in 1987, and the M.S. degree in Computer Engineering from Loyola College in 1989. He has been with the Laser Remote Sensing Branch of the Laboratory for Terrestrial Physics at NASA Goddard Space Flight Center, Greenbelt, MD since 1989 where he has worked on several airborne and spaceborne LIDARS. He was the flight software lead and worked on the operational algorithms for the Mars Orbiter Laser Altimeter (MOLA). He is currently the Instrument Scientist for the Vegetation Canopy Lidar (VCL) and the Principal Investigator for the Laser Vegetation Imaging Sensor (LVIS) and leads the waveform algorithm development teams for these instrument. His interests include development of new laser altimeter techniques to allow wide-swath mapping and eventually mapping from spaceborne instruments. He has worked for the last 8 years on algorithms and techniques for analysis of laser altimeter return waveforms for vegetation measurements, topographic change detection, and the production of highly accurate digital elevation models.

Fig. 1. (a) Simple and (b) complex laser altimeter return waveforms, collected by the Laser Vegetation Imaging Sensor (LVIS) airborne altimeter system. The waveform represents the distribution of light reflected from all intercepted surfaces within the footprint. The positions of the peak amplitude and centroid of the waveform are shown by solid and dashed lines respectively. These are calculated using all data above the background noise level.

Fig. 2. Simulated complex laser altimeter return waveform before (solid line) and after smoothing using a Gaussian of half-width 5, 10 and 15 bins respectively (dashed lines). The simulated waveform was generated from the sum of three Gaussians, each with position, amplitude and half-width parameters of (193.76, 35.53, 20.63), (257.21, 15.28, 10.00), and (305.20, 41.12, 2.80) respectively.

Fig. 3. (a) Simulated and approximated return laser altimeter waveform after optimization, and (b) the difference between the two.

Fig. 4. (a) Locations of places referred to in the text, and (b) a schematic showing the LVIS flight configuration. The laser scans from side to side as the airplane moves forward. (c) Geolocated LVIS footprints in the Sequoia National Forest, CA, from an East-West oriented flight in October 1997. The footprint locations are denoted by a cross. Footprints are ~25 m in diameter. The aircraft ground track is shown by the solid line across the center of the data swath. The locations of footprints whose waveforms are discussed in the text are denoted by asterisks.

Fig. 5. Digitized LVIS laser (a) output and (b) return pulses (solid lines) and their Gaussian components (dashed lines) from the Sequoia National Forest, CA, obtained using the waveform decomposition algorithm.

Fig. 6. Vertically-geolocated waveforms (relative to the WGS-84 ellipsoid) for the footprints highlighted in Fig. 4c. The Gaussian components, determined using the decomposition algorithm, are shown using solid lines. The dashed horizontal lines indicate the elevations at which component Gaussians locate reflecting surfaces in at least two consecutive footprints, as determined by the locations of these Gaussians.

TABLE I

INITIAL PARAMETER VALUES FOR THE GAUSSIAN COMPONENTS DETECTED WITHIN THE SIMULATED LASER ALTIMETER RETURN WAVEFORM SHOWN IN FIG. 2. GAUSSIANS 9–11 MEET THE INITIAL FLAGGING CRITERIA AND THUS ARE THE ONLY ONES USED INITIALLY IN THE OPTIMIZATION. IF THE PRESCRIBED DATA ACCURACY IS NOT MET, THE REMAINING GAUSSIANS ARE INCLUDED IN THE OPTIMIZATION ACCORDING TO THEIR RANK.

Gaussian	Position	Amplitude	Half-width	Rank
1	6.50	0.11	3.50	9
2	18.50	0.10	1.50	8
3	32.00	0.34	4.00	7
4	49.50	0.53	5.50	6
5	69.50	0.08	6.50	5
6	90.50	0.06	4.50	4
7	107.00	0.11	5.00	3
8	125.50	0.00	3.50	2
9	192.50	34.29	21.50	
10	257.50	14.30	10.50	
11	304.00	27.30	5.00	
12	335.00	0.32	4.00	1

TABLE II

INITIAL AND OPTIMIZED PARAMETER VALUES FOR THE COMPONENT GAUSSIANS FLAGGED AS "IMPORTANT" IN STEP C. THE ACTUAL PARAMETERS OF THE THREE GAUSSIANS USED TO GENERATE THE SIMULATED LASER ALTIMETER RETURN WAVEFORM SHOWN IN FIG. 2 ARE SHOWN FOR COMPARISON.

Value	x_1	a_1	σ_1	x_2	a_2	σ_2	x_3	a_3	σ_3	m
Initial	192.50	34.29	21.50	257.50	14.30	10.50	304.00	27.30	5.00	7.09
Optimized	194.01	35.38	20.30	257.16	14.83	10.01	305.15	42.21	2.65	7.08
Actual	193.76	35.52	20.63	257.21	15.28	10.00	305.20	41.12	2.80	7.07

TABLE III

GAUSSIAN COMPONENTS OF THE WAVEFORM SHOWN IN FIG. 5B. THE POSITION, HALF-WIDTH AND AMPLITUDE OF THE *ith* GAUSSIAN COMPONENT ARE DENOTED BY x_i, σ_i, AND a_i RESPECTIVELY.

Gaussian	x_i (bins)	σ_i (bins)	a_i (counts)
1	72.72	6.20	8.14
2	98.57	9.91	10.50
3	144.30	11.47	9.21
4	183.97	12.97	11.26
5	301.38	3.20	14.62